A model to predict the s-phase thickness and the change in corrosion behavior toward H$_2$SO$_4$ of 316L austenitic stainless steel after plasma nitriding

Phillip Marvin Reinders [*], Günter Bräuer

Technische Universität Braunschweig, Institute for Surface Technology, Riedenkamp 2, 38106 Braunschweig, Germany

ABSTRACT

Austenitic steels are known for their high corrosion resistance, but at the same time exhibit low hardness and wear resistance. While plasma nitriding improves tribological properties, it also affects corrosion behavior depending on the electrolyte. In this paper, a model should be present, that allows to predict the thickness of the s-Phase and the change of the corrosion behavior in plasma nitriding processes for austenitic stainless steels. For this purpose, different processes under specific variation of the temperature ranging from 360 °C to 450 °C and duration of 10 h to 24 h were performed. Other process parameters such as the voltage or gas mixture remained constant. There are two stages in the developed model: the first one allows the prediction of the s-Phase thickness by isothickness curves. The second stage implements an evaluation system of the corrosion resistance. By assigning numerical values for the observed corrosion, a quantitative comparison is allowed, which is represented by a color scaling.

1. Introduction

Austenitic stainless steels (ASS) are used in several fields of applications due to their excellent corrosion resistance. These include pipelines in the chemical and food industries [1–3], as tools or implants in medical technology [4,5] or, with increasing interest, as a material for metallic bipolar plates in fuel cells, to name a few [6–8].

Responsible for the excellent corrosion resistance of ASS is the chromium oxide layer, which is caused by the high free chromium content in the iron matrix. In contact with oxygen contained in the surrounding medium, chromium forms a thin passive layer, which has a strong diffusion-inhibiting effect [9]. However, in addition to the electrically isolating passive layer, ASS also exhibit low hardness and therefore low wear resistance, which limits further potential applications [8,10–12].

The tribological properties of austenitic stainless steels can be improved by thermochemical surface treatment, such as plasma nitriding. By enriching the surface layer with nitrogen above the solubility limit (up to 30 at. %), a strong lattice distortion occurs and thus the metastable expanded austenite is formed, the so-called s-Phase [2,13].

There are contrasting reports in the literature on the simultaneously improvement of both properties (tribological and corrosive) by plasma nitriding, which can be attributed to strongly different corrosive conditions, such as the composition of the electrolyte, temperature or more complex interactions between material and stress. In general, the formation of chromium nitrides has to be suppressed to provide sufficient free chromium in the iron matrix for the formation of the passive layer [2,14,15].

There are various process parameters that influence the diffusion behavior and the formation of the s-Phase. This also includes the chemical composition of the steel, the microstructure and defects, as well as the roughness and surface pretreatment. All these influences already have been extensively studied by various authors. For example, Łępicka et al. [16] have shown that the chemical composition has an influence not only on the corrosion resistance, but also on the diffusion depth. Chemkhi et al. [17,18] were able to show that the properties depend significantly on the surface pretreatment. A good summary is given by [2]. However, the most investigated parameters in the literature are focused on treatment temperature and duration, whereas other process parameters such as gas composition [19] or pressure [20,21] are less studied. Nevertheless, the influence of these parameters cannot be neglected, as nitrogen content in the process gas, pressure, voltage and pulse pause are important to control how much diffusible nitrogen can be made available for the formation of the s-Phase. Typical values for

Table 1

Chemical composition of AISI 304L austenitic stainless steel in weight percentage.

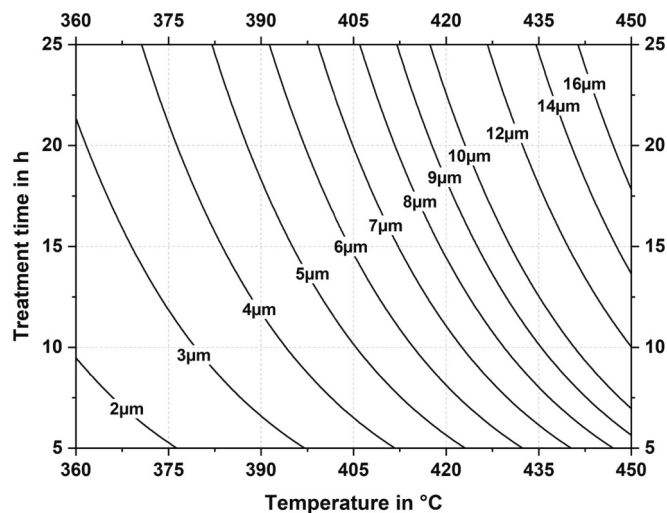| C	Si	Mn	Ni	Cr	Mo	N	S	P	Co	Fe
0.026	0.51	1.32	10.15	16.66	2.04	0.038	0.003	0.033	0.212	Balance

Fig. 1. Iso-thicknesslines for 316L.

low-temperature treatments vary from 300 to a maximum of 450 °C, depending on the literature, noting that the treatment duration should be shorter at higher temperatures [13,19,22,23]. But as mentioned before, material-specific influences such as the chemical composition and the microstructure of the ASS cannot or must not be neglected, as shown e. g. by Musekamp et al. [9]. Therefore, the maintenance of corrosion resistance of plasma nitrided ASS still is a problem for the simultaneous optimization of both properties and hence the selection of nitriding treatment parameters.

There are already some approaches in the literature, that deal with the change in corrosion resistance as a function of process temperature and duration, refer to [13], that can be traced back to the work of Sun and Bell [24,25]. However, these approaches are limited to a threshold, e. g., a corrosion current density, and were finally not continued.

Based on the above-mentioned preliminary work and the conflicting targets of wear protection and corrosion resistance, a new, extended model will be described in the present work. On the one hand, the model allows to predict the thickness of the s-Phase under given treatment parameters. On the other hand, it describes the quantitative change of the corrosion resistance in sulfuric acid. With this approach the user is able to decide how much wear protection he will obtain at the expense of the corrosion resistance, or how much he can achieve at maximum without significant change of it. In this way, the industry is provided with a tool that allows it to obtain reproducible results at specific treatment intervals. The development of the model was done in two steps. A detailed description of the determination of the s-Phase thickness as a function of the process parameters can be found in [26,27] and therefore only briefly will be mentioned in the following.

2. Material and methods

For this study, identical samples of 316L as in the previous investigation [27] were used. Therefore, details about the sample preparation, the process management during plasma nitriding as well as the metallographic preparation can be found in [26,27]. Only the chemical composition is listed for the purpose of completeness (Table 1).

In the first stage of the model [26], 304L austenitic stainless steel was used in the solution-annealed and polished condition. A total of 14

different plasma nitriding treatments were performed under the variation of treatment temperature and duration. Since there are many influencing variables on the nitriding result, as already mentioned, the model is initially limited to two influencing factors and the remaining process parameters were kept constant. Afterwards, temperature-dependent slopes were determined by means of the s-Phase thicknesses, which allowed to determine an s-Phase formation coefficient. Using this, a formulaic relationship was built that allows to plot arrays of curves of equal s-Phase thicknesses to be plotted as a function of treatment temperature and duration. An example is shown in Fig. 1. In a second step, we transferred the results of the 304 L from [26] to different austenitic steels e. g. 316 L [27], which was followed up in this work.

At this point, the previously published model is extended to include statements on corrosion resistance, correlating the interactions of the process parameters with the properties and thus enabling optimization of both target goals. Since the evaluation of corrosion resistance is a complex topic with a large number of influencing factors, limitations must be made at this point.

Since most cases of metal corrosion occur through an electrochemical reaction at the interface, potentiodynamic measurements will be considered for this study. While this analysis does not consider long-term stability, it can provide information on the behavior of the material with respect to corrosion tendency and rate. Typically, these values are obtained by the Tafel plot. Details can be found in the technical literature, e. g. [28].

Potentiodynamic measurements were performed using a conventional three-electrode system, with the specimen acting as the working electrode, graphite electrodes, and a saturated Hg/Hg_2SO_4 electrode as counter and reference electrodes, respectively. A potentiostat (Autolab PGSTAT204) from Metrohm with the Nova evaluation software was used. The measurements themselves were made following the DOE2022 [29] in order to investigate the potential of the treatment for the bipolar plate in more detail. To achieve a distinct differentiation between the experimental parameters and to enable a comparison with values from the literature, the electrolyte and the scanning rate were adjusted. The exact parameters are the following: open-circuit potential for 1 h under simultaneous heating of 0.05 M sulfuric acid to 80 °C in an interval of −1.2 to 1.2 V (−0.56 to 1.84 vs SHE) with a scan rate of 1 mV/s and a step size of 10 mV, purged under air (cathodic environment).

In addition to data from literature gained by the conventional investigations, this work not only references on the Tafel analysis to make conclusions about the change in corrosion behavior. The model presented also provides area units in order to evaluate voltage ranges as they are passed through in the bipolar plate.

3. Modelling and discussion

In order to determine the change in corrosion behavior numerically with different evaluation criteria and to describe it by means of an individual weighting, the following formula (1) was developed:

$$CRV_{treat}(x) = A*\big(CRV_{Ref} + B*x_B + C*x_C\big) \tag{1}$$

[+] CRV_{treat}: Corrosion Resistance Value of a treated specimen.
[+] CRV_{Ref}: Corrosion Resistance Value of an untreated specimen.
[+] A: Maximum corrosion rate.
[+] B: Shift of the corrosion potential.
[+] C: Area current density in a defined interval (here from 0 to 1 V).
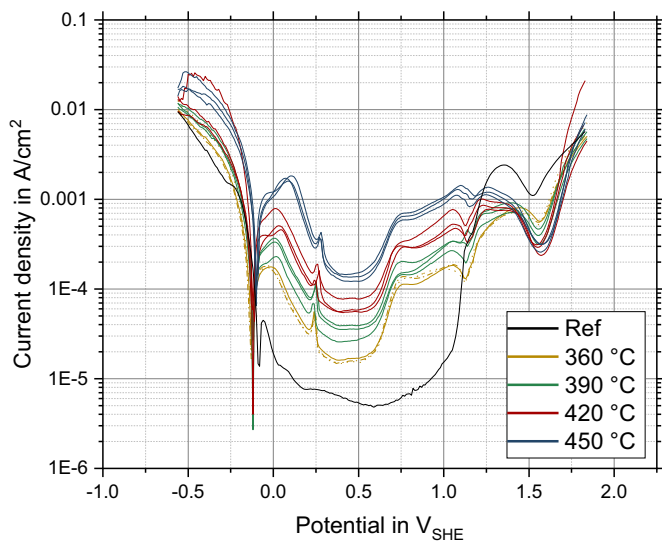[+] x_B/x_C: Weighting factors.

Fig. 2. Selected potentiodynamic measurement curves with one color indicates one process temperature.

Table 2
Electrochemical parameters extracted from potentiodynamic curves of 316L in H_2SO_4 solution.

Treatment parameters (°C / h)	$I_{corr}/\mu A \cdot cm^{-2}$	E_{corr}/V_{SHE}
Ref	6.135	−0.774
360/16	13.87	−0.130
360/20	15.09	−0.137
360/24	22.18	−0.130
390/10	26.39	−0.135
390/12	23.38	−0.137
390/16	26.54	−0.126
390/20	50.77	−0.119
390/24	87.99	−0.133
420/10	75.77	−0.120
420/12	51.61	−0.121
420/16	135.90	−0.127
450/10	106.00	−0.106
450/12	132.98	−0.100
450/16	201.37	−0.105

The corrosion resistance value of a treated sample (CRV_{treat}) is a function of the corrosion resistance value of an untreated sample (CRV_{Ref}) as well as the change based on various factors (A, B, C), which will be described in detail below. The equation is designed in a way that values for CRV_{treat} greater than 100 represent an improvement, whereas values less than 100 describe a decline of the corrosion resistance. Therefore, CRV_{Ref} has an initial value of 100 in this work. It is important to note that the formula is only valid for austenitic stainless steels with the same curve shape.

3.1. A: Maximum corrosion rate

This factor is related to the corrosion current I_{corr}, which allows conclusions about the corrosion kinetics. It can be determined using the Tafel plot. If I_{corr} is greater than a defined threshold value, A and thus the whole term becomes zero. Otherwise it takes the value one. Currently, the factor can be understood as a kind of filter, which ensures that the curves, which exceed a desired value, are not considered. In this work, we have set the value for the filter to 205 $\mu A \cdot cm^{-2}$ on purpose, so all data are included in the visualization of the model. Fig. 2 shows selected potentiodynamic measurement curves, where one color indicates a process temperature. For reasons of clarity, a detailed legend has been omitted. The corrosion current density of the individual measurements

is given in Table 2.

3.2. B: Corrosion potential

The corrosion potential E_{corr}, which is also determined by the Tafel straight line, provides information about the corrosion tendency of the material. The shift of the corrosion potential E_{corr} in a more positive direction represents a nobler electrode potential. To determine the shift, a database was built that automatically processes the current and future data sets using Phyton scripts and then visualizes them with Grafana.

The shift is calculated by simply subtracting the corrosion potential of the reference (E_{Ref}) from the corrosion potential to be evaluated (E_{Eva}). The reference potential does not necessarily have to be the data set of a reference, it can also represent an adapted treatment. In this way, different surface treatments can be compared with each other as well as the deviation within same surface treatments.

For example, if the evaluating potential has a more positive value than the reference potential, the surface is nobler and a positive result is obtained. However, if the reference potential is higher, the result is negative which can be assigned to degradation. To evaluate this shift quantitatively, a linear fit can be used, where the shift serves as the variable of a function and the function value itself corresponds to the evaluation points. The allocation of evaluation points is linked by setting a maximum allowable shift and a query that allows a maximum deduction of 100 points. This is represented by Eq. (2):

$$B = \frac{(E_{Eva} - E_{Ref})*100}{a} \tag{2}$$

The parameter a describes a desired interval to be considered (e.g. from 0.3 V).

In case the shift of the corrosion potential should not be considered, e.g. because the variations in austenitic stainless steels are too large under different basic conditions (electrolyte, scan speed, etc.) [30], the weighting factor x_B can be set to zero. Table 2 shows the values of E_{corr}.

3.3. C: Area current density in a defined interval

This factor is a new defined variable. The above-mentioned DOE2022 [29] specifies certain potential ranges for the electrochemical testing of bipolar plates, which are also passed through during operation. These intervals are therefore also included in the consideration for the description of the corrosion resistance. The calculations for this parameter were carried out as described for the corrosion potential B using Phyton scripts and Grafana.

At first, the scripts calculate the mathematical area of each individual curve at a selected interval. Integration along the given axis was done using the compound trapezoidal rule. In this work the interval is set from 0 to 1 V. The next step is to determine the area ratios between the different curves. Furthermore, the area ratios among each other are determined by choosing a data set as a reference value. Once again, the reference data set does not necessarily have to be the data set of a reference, if different surface treatments are compared with each other. The relation is formed from the reference data set to the data set to be evaluated and serves as a variable for the subsequent fit, whereas the function value should correspond to the evaluation points of the factor.

Since the area ratios can take on very different values in their dimensions, linear scaling, as it was the case with the "Corrosion potential" factor, it is not suitable. With linear scaling, small changes are very quickly suppressed in the noise compared to large values. As a result, the marginal influences are underestimated and not perceived. Similar results are obtained with potential functions.

A fit function became necessary, which clearly shows small changes of the relation, does not overestimate moderate values and approximates large relations to a maximum. Logarithmic and root functions allow a pronounced representation of small relations and limit large relations,
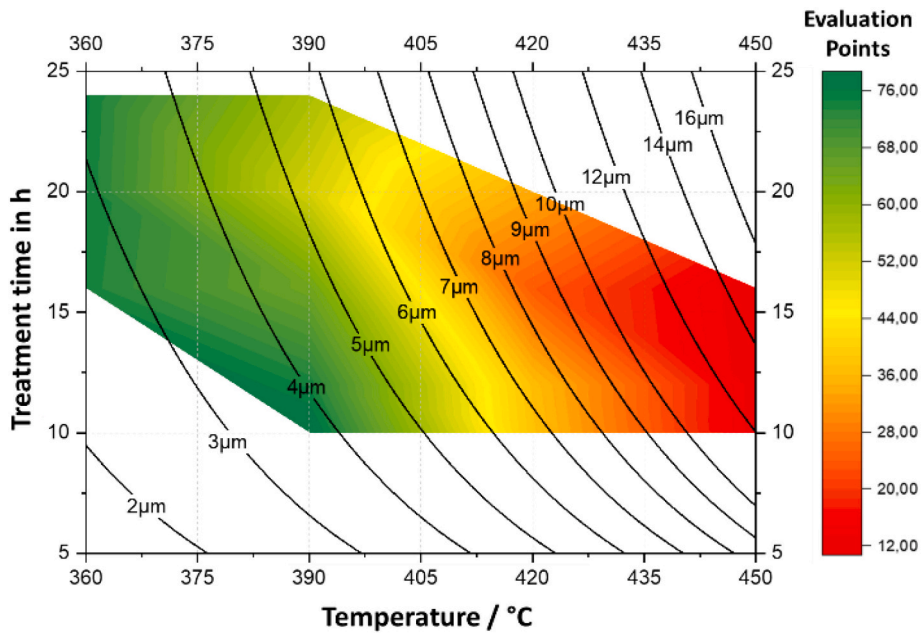
Fig. 3. Combined plot of s-Phase thickness and corrosion resistance as a function of treatment temperature and duration. With the weights $x_B = 0.1$, $x_C = 0.9$ $a = 0.3$ und $b = 0.08$.

but fail in the interpretation of values below zero, i.e. where the data to be evaluated is smaller than the reference data.

To fulfill the requirements from above, a suitable function is the sigmoid function. This function is generally described by Eq. (3).

$$S(x) = \frac{1}{1 + e^{-x}} \tag{3}$$

In order for the function to fit the data in the model as closely as possible, some adjustments are necessary. To return the maximum evaluation points (100 in this case) for the expression "Area current density in a defined interval", the function must converge to this value. Secondly, the function must pass through the origin, since no change in corrosion behavior occurs for the relation value equal to one, and thus the function takes the value zero. Third, the function must be stretched to the maximum relation, which may change depending on the selected data to be evaluated. Finally, the function must be multiplied by minus to return negative values at higher relations. With these boundary conditions, Eq. (3) changes to Eq. (4).

$$C = S'(x) = 100 - \left(\frac{200}{1 + e^{-bx}} \right) \tag{4}$$

The parameter b can be used to fit the data in a way that the maximum relation achieves 100 evaluation points. The fitting parameter can either be calculated automatically by using the database to select the curves of interest, or it can be approximated manually until the desired spread is achieved. For the processes performed in [15], b = 0.08 gives a very good approximation. For relations smaller than 1, the ratio of the reference to the to be evaluated has to be reversed in order to use the evaluation points on full scale. The query is controlled by a case query of type When-Then in the scripts.

3.4. Merging of the models

Using the three described expressions and the personalized weighting, the CRVtreat can be calculated for each plasma nitration process. Implemented as an additional axis in the model from [15] the following graph is obtained (Fig. 3).

The presented model allows the simultaneous analysis of the s-Phase thickness - as a dimension of the wear resistance - and the change in the

corrosion behavior as a function of the treatment temperature and duration. However, this does not mean that the thickness of the s-Phase is functionally related to corrosion resistance, but that the properties of corrosion resistance and s-Phase thickness are influenced by the process parameters of temperature and treatment time with different degrees of intensity. Fig. 3 illustrates this, for example, for an s-Phase thickness of 6 μm, at which CRV of approx. 44 to 56 are achieved.

The user is thus enabled to estimate the desired target values in advance and to weigh them accordingly. For example, it is possible to determine the amount of the wear protection (s-Phase thickness) at the expense of corrosion resistance. To make the evaluation more individual, it is possible for each user to add further terms or expressions. For example, if the corrosion type is a decisive factor, e. g. pitting. Since the model is based on a database, a sharp rise followed by a fall in the current density curve can be detected and reported accordingly through data retrieval and analysis. Also, a quick and individual adjustment also is possible, e. g. by weighting or changing the reference value.

However, since the evaluation of corrosion resistance is based purely on the electrochemical characterization, especially the potentiodynamic measurements, this model only provides an initial estimate. Additional corrosion analyses as well as the evaluation under very complex real conditions can't be represented so far. Moreover, only the two most influencing treatment parameters were considered in the model. The implementation of further process parameters or different microstructures is very complex and subject to future investigations.

4. Conclusions

In the present work, a model was developed which allows to estimate the surface properties of ASS after plasma nitriding depending on the treatment temperature and duration in advance. The model is based on the preliminary investigations from [26,27] and was enhanced with a calculation procedure for the change in corrosion behavior.

For this purpose, potentiodynamic polarization curves were used to determine the typical characteristic values for corrosion evaluation by means of a Tafel plot, on the one hand, and to enable the area ratios to be changed in a freely selectable potential interval, on the other. The determined area ratios were fitted with an adapted sigmoid function in order to assign a numerical value to the respective relations. Using a

formulaic relationship, the corrosion potential and the change in area ratios were weighted and converted into a corrosion resistance value. This value then was visualized and allows the user to estimate the amount of the wear protection or corrosion resistance to be achieved at the expense of the other property.

CRediT authorship contribution statement

Phillip Marvin Reinders: Conceptualization, Methodology, Software, Validation, Formal analysis, Investigation, Data curation, Writing – original draft, Visualization, Project administration, Funding acquisition. **Günter Bräuer:** Conceptualization, Resources, Writing – review & editing, Supervision, Funding acquisition.

Declaration of competing interest

Data availability

The data that has been used is confidential.

Acknowledgement

References

[1] M. Keddam, T. Thiriet, G. Marcos, T. Czerwiec, Characterization of the expanded austenite developed on AISI 316 LM steel by plasma nitriding, J Min Metall B Metall 53 (2017) 47–52, https://doi.org/10.2298/JMMB151115026K.

[2] F. Borgioli, The corrosion behavior in different environments of austenitic stainless steels subjected to thermochemical surface treatments at low temperatures: an overview, Metals 13 (2023) 776, https://doi.org/10.3390/met13040776.

[3] P. Cisquini, S.V. Ramos, P.R.P. Viana, V.D.F.C. Lins, A.R. Franco, E.A. Vieira, Effect of the roughness produced by plasma nitrocarburizing on corrosion resistance of AISI 304 austenitic stainless steel, J. Mater. Res. Technol. 8 (2019) 1897–1906, https://doi.org/10.1016/j.jmrt.2019.01.006.

[4] F. Borgioli, E. Galvanetto, T. Bacci, Surface modification of austenitic stainless steel by means of low pressure glow-discharge treatments with nitrogen, Coatings 9 (2019) 604, https://doi.org/10.3390/coatings9100604.

[5] X.Y. Li, Y. Sun, T. Bell, Stability of the nitrogen S-phase in austenitic stainless steel, Metallurgy and Materials (1999) 901–907.

[6] K. Lin, X. Li, L. Tian, H. Dong, Active screen plasma surface co-alloying of 316 austenitic stainless steel with both nitrogen and niobium for the application of bipolar plates in proton exchange membrane fuel cells, Int. J. Hydrogen Energy 40 (2015) 10281–10292, https://doi.org/10.1016/j.ijhydene.2015.06.010.

[7] D.P. Davis, P.L. Adcock, M. Turpin, S.J. Rowen, Bipolar plate materials for solid polymer fuel cells, J. Appl. Electrochem. (2000) 101–105.

[8] S. Pugal Mani, N. Rajendran, Corrosion and interfacial contact resistance behavior of electrochemically nitrided 316L SS bipolar plates for proton exchange membrane fuel cells, Energy 133 (2017) 1050–1062, https://doi.org/10.1016/j.energy.2017.05.086.

[9] J. Musekamp, H. Hoche, T. Schmitt, P.-M. Reinders, M. Oechsner, P. Kästner, G. Bräuer, Influence of material condition and chemical composition on the

[10] D.D. Papadias, R.K. Ahluwalia, J.K. Thomson, H.M. Meyer, M.P. Brady, H. Wang, J. A. Turner, R. Mukundan, R. Borup, Degradation of SS316 bipolar plates in simulated fuel cell environment: corrosion rate, barrier film formation kinetics and contact resistance, J. Power Sources 273 (2015) 1237 1249, https://doi.org/10.1016/j.jpowsour.2014.02.053.

[11] M. Xu, S. Kang, J. Lu, X. Yan, T. Chen, Z. Wang, Properties of a plasma-Nitrided coating and a CrNx coating on the stainless steel bipolar plate of PEMFC, Coatings 10 (2020) 183, https://doi.org/10.3390/coatings10020183.

[12] E.M. Gabreab, G. Hinds, S. Fearn, D. Hodgson, J. Millichamp, P.R. Shearing, D. J. Brett, An electrochemical treatment to improve corrosion and contact resistance of stainless steel bipolar plates used in polymer electrolyte fuel cells, J. Power Sources 245 (2014) 1014–1026, https://doi.org/10.1016/j.jpowsour.2013.07.041.

[13] H.-J. Spies, C. Eckstein, H. Biermann, A. Franke, Corrosion behaviour of stainless steels after low temperature thermochemical treatment, Mat.-wiss. u. Werkstofftech. 41 (2010) 133–141, https://doi.org/10.1002/mawe.201000563.

[14] F. Borgioli, E. Galvanetto, T. Bacci, Low temperature nitriding of AISI 300 and 200 series austenitic stainless steels, Vacuum 127 (2016) 51–60, https://doi.org/10.1016/j.vacuum.2016.02.009.

[15] M. Olzon-Dionysio, S.D. de Souza, R. Basso, S. de Souza, Application of Mössbauer spectroscopy to the study of corrosion resistance in NaCl solution of plasma nitrided AISI 316L stainless steel, Surf. Coat. Technol. 202 (2008) 3607–3614, https://doi.org/10.1016/j.surfcoat.2007.12.040.

[16] M. Łepicka, M. Grądzka-Dahlke, Direct current and pulsed direct current plasma nitriding of ferrous materials a critical review, Acta Mechanica et Automatica 10 (2016) 150–158, https://doi.org/10.1515/ama-2016-0024.

[17] M. Chemkhi, D. Retraint, A. Roos, C. Garnier, L. Waltz, C. Demangel, G. Proust, The effect of surface mechanical attrition treatment on low temperature plasma nitriding of an austenitic stainless steel, Surf. Coat. Technol. 221 (2013) 191–195, https://doi.org/10.1016/j.surfcoat.2013.01.047.

[18] M. Chemkhi, D. Retraint, A. Roos, C. Demangel, Role and effect of mechanical polishing on the enhancement of the duplex mechanical attrition/plasma nitriding treatment of AISI 316L steel, Surf. Coat. Technol. 325 (2017) 454–461, https://doi.org/10.1016/j.surfcoat.2017.06.052.

[19] E. de Las Heras, G. Ybarra, D. Lamas, A. Cabo, E.L. Dalibon, S.P. Brühl, Plasma nitriding of 316L stainless steel in two different N2-H2 atmospheres - influence on microstructure and corrosion resistance, Surf. Coat. Technol. 313 (2017) 47–54, https://doi.org/10.1016/j.surfcoat.2017.01.037.

[20] F. Borgioli, A. Fossati, E. Galvanetto, T. Bacci, G. Pradelli, Glow discharge nitriding of AISI 316L austenitic stainless steel: influence of treatment pressure, Surf. Coat. Technol. 200 (2006) 5505–5513, https://doi.org/10.1016/j.surfcoat.2005.07.073.

[21] M. Campos, S. de Souza, J.P. Davim, S.D. de Souza, M. Olzon-Dionysio, Influence of the gas pressure of plasma nitriding on the structural, mechanical and Tribological surface properties of AISI 316L, Mat. Res. 22 (2019), https://doi.org/10.1590/1980-5373-mr-2019-0302.

[22] I. Flis-Kabulska, Y. Sun, J. Flis, Monitoring the near-surface pH to probe the role of nitrogen in corrosion behaviour of low-temperature plasma nitrided 316L stainless steel, Electrochim. Acta 104 (2013) 208 215, https://doi.org/10.1016/j.electacta.2013.04.111.

[23] E.A. Bernardelli, P.C. Borges, Fontana L. C., J.B. Floriano, Role of plasma nitriding temperature and time in the behaviour and microstructure evolution of 15-5 PH stainless steel, Kovove Mater. 2010 (2009) 105–115.

[24] Y. Sun, Kinetics of low temperature plasma carburizing of austenitic stainless steels, J. Mater. Process. Technol. 168 (2005) 189–194, https://doi.org/10.1016/j.jmatprotec.2004.10.005.

[25] R. Tian, J. Sun, L. Wang, Plasma-nitrided austenitic stainless steel 316L as bipolar plate for PEMFC, Int. J. Hydrogen Energy 31 (2006) 1874–1878, https://doi.org/10.1016/j.ijhydene.2006.03.003.

[26] P.M. Reinders, R.R. Patel, J. Musekamp, P. Kaestner, H. Hoche, G. Bräuer, M. Oechsner, Determination of the s-phase formation coefficient of plasma nitrided austenitic steel, Materialwiss. Werkstofftech. 52 (2021) 193–201, https://doi.org/10.1002/mawe.202000029.

[27] P.M. Reinders, R.R. Patel, P. Kaestner, G. Bräuer, Ein Diffusionsmodell für Plasmanitrierprozesse austenitischer Stähle, Vakuum in Forschung und Praxis 32 (2020) 38–41, https://doi.org/10.1002/vipr.202000750.

[28] R.A. Cottis, L.L. Shreir, Shreir's Corrosion, 4th ed., Elsevier, Amsterdam, London, 2010.

[29] U.S. Department Of Energy, DOE Technical Targets for Polymer Electrolyte Membrane Fuel Cell Components: Hydrogen and Fuel Cell Technologies Office, https://www.energy.gov/eere/fuelcells/doe-technical-targets-polymer-electrolyte-membrane-fuel-cell-components, accessed 13 April 2023.

[30] Y.X. Qiao, Y.G. Zheng, P.C. Okafor, W. Ke, Electrochemical behaviour of high nitrogen bearing stainless steel in acidic chloride solution: effects of oxygen, acid concentration and surface roughness, Electrochim. Acta 54 (2009) 2298–2304, https://doi.org/10.1016/j.electacta.2008.10.038.